Progress In Electromagnetics Research, Vol. 114, 67–88, 2011

THEORETICAL FOUNDATION FOR THE METHOD OF CONNECTED LOCAL FIELDS

S.-Y. Mu and H.-W. Chang

Institute of Electro-optical Engineering and Department of Photonics National Sun Yat-sen University, Kaohsiung 80424, Taiwan, R.O.C.

Abstract—The method of connected local fields (CLF), developed for computing numerical solutions of the two-dimensional (2-D) Helmholtz equation, is capable of advancing existing frequency-domain finite-difference (FD-FD) methods by reducing the spatial sampling density nearly to the theoretical limit of two points per wavelength. In this paper, we show that the core theory of CLF is the result of applying the uniqueness theorem to local EM waves. Furthermore, the mathematical process for computing the local field expansion (LFE) coefficients from eight adjacent points on a square is similar to that in the theory of discrete Fourier transform. We also present a theoretical analysis of both the local and global errors in the theory of connected local fields and provide closed-form expressions for these errors.

1. INTRODUCTION

Recently we presented a method called connected local fields (CLF) [1–4] which was developed for obtaining numerical solutions of the Helmholtz equation in a homogeneous, and ultimately, an inhomogeneous medium. The method started with a Fourier-Bessel series expansion of a local field defined over a square patch consisting of nine points arranged as shown in Figure 1. From these Fourier-Bessel coefficients we derived FD-like, compact nine-point stencils for the 2D Helmholtz equation. We show that CLF is capable of advancing existing FD-FD methods [5–9] by reducing the sampling density to just a little more than two points per wavelength, which is theoretical limit for spatial sampling.

In this paper we will derive a closed-form expression for the error characteristics in both LFE-5 and LFE-9 algorithms. The

Received 14 December 2010, Accepted 15 February 2011, Scheduled 18 February 2011
Corresponding author: Hung-Wen Chang (hchang@faculty.nsysu.edu.tw).

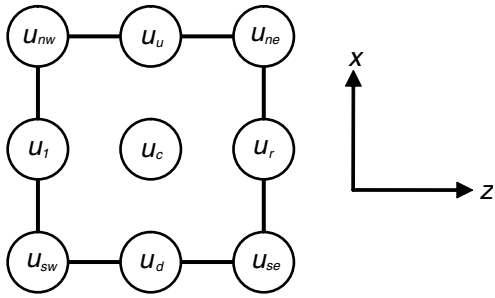

Figure 1. The basic square patch centered at a point u_c and its adjacent nodes.

relation between the theory of CLF and the uniqueness theorem in electromagnetic waves will also be investigated. We show that CLF is the result of applying the (modified) theory of discrete Fourier Transformation to the uniqueness theorem. We hope, by the end of this work, readers shall have a better understanding of how and why the method of connected local fields works.

2. LFE EQUATIONS FOR THE HELMHOLTZ EQUATION

First we summarize the main results of Ref. [1] upon which we shall investigate their error characteristics. The theory of CLF for 1-D Helmholtz equation is stated as followed: A point u_0 is related to its two neighbors u_{-1}, u_1, by:

$$u_0 = \frac{1}{2\cos(k\Delta)}u_{-1} + \frac{1}{2\cos(k\Delta)}u_1, \tag{1}$$

where k is the wavenumber, Δ is the spacing between points. Note that Equation (1) is exact. Next, for 2D cases, we have LFE-5 and LFE-9 formulations. The following are the plus and the cross version in the LFE-5 case:

$$u_c = \frac{u_r + u_u + u_l + u_d}{4J_0(V)}, \quad \text{(LFE-5+)} \tag{2}$$

and

$$u_c = \frac{u_{ne} + u_{nw} + u_{se} + u_{sw}}{4J_0(\sqrt{2}V)}. \quad \text{(LFE-5X)} \tag{3}$$

Here $V = k\Delta$ is the normalized frequency. The advantage of LFE-5+ formulation is that by simply upgrading old coefficients to new corresponding coefficients in Equation (2), it can improve the accuracy of all existing five-point FD-FD programs without changing the

existing program structures. Currently, we have no direct application of the LFE-5X formulation by itself. In Section 4.2, we show that both LFE-5 equations can be used to provide an alternate derivation for the following LFE-9 equation:

$$u_c = \frac{1}{4}\frac{J_4(\sqrt{2}V)\cdot(u_r+u_u+u_l+u_d)+J_4(V)\cdot(u_{ne}+u_{nw}+u_{se}+u_{sw})}{J_0(V)\cdot J_4(\sqrt{2}V)+J_0(\sqrt{2}V)\cdot J_4(V)}, \text{ (LFE-9)} \quad (4)$$

We show in Ref. [1] that this LFE-9 equation leads to an improved compact nine-point FD-FD stencil for the 2-D homogeneous Helmholtz equation. It would help advance all existing FD-FD methods by reducing much needed computational resources without sacrificing accuracy.

3. LFE-9 FROM UNIQUENESS THEOREM AND DISCRET FOURIER TRANSFORM

In this section we will study the relationship between theory of connected local fields and the uniqueness theorem. We show that LFE-9 equation is the "digital" realization of the uniqueness theorem via discrete Fourier transform.

3.1. The Uniqueness Theorem for the Helmholtz Equation

Consider volume **V**, surrounded by surface **S**, the uniqueness theorem [10–12] of the Maxwell equations states that the necessary and sufficient conditions for the time-harmonic EM field inside **V** to be uniquely specified within **S**. Only one of the following three conditions is needed for the theorem to hold true:

1. The tangential electric field is specified on **S**.
2. The tangential magnetic field is specified on **S**.
3. The tangential electric field is specified on part of the surface **S** and the tangential magnetic field specified on the rest of the surface **S**.

In the 2-D case, the uniqueness theorem states that if either the tangential electric or the magnetic fields, is specified on the aerial perimeter (but not both simultaneously), the field within the area will be completely determined.

3.2. Digitizing the Uniqueness Theorem and the Perimetric Sampling Density

Figure 2 shows a standard 2-D FD grid layout with two squares enclosing u_c. Note that $C1$ is the inner square with eight points on

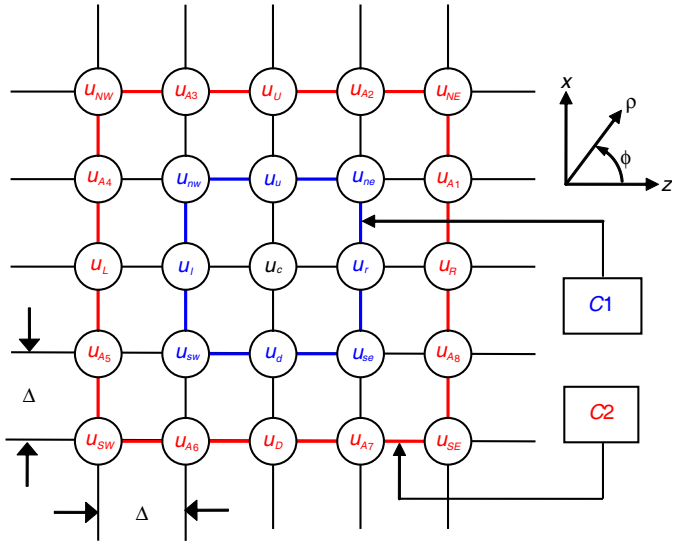

Figure 2. A layout of a two-dimensional grids showing the centered point u_c and two squares $C1$ and $C2$ enclosing the reference point.

the perimeter (shown in blue) while $C2$, the outer square, has sixteen points on its boundaries (shown in red). Let us apply the uniqueness theorem to the square patches of Figure 2. Strictly speaking, in order to uniquely determine the fields inside this boxed ring, we must specify the fields for every point on the square perimeter. In other words, we need infinite perimetric resolution to fulfill the uniqueness theorem. In the field of digital signal processing we have the sampling theorem to convert data between the analog and digital world. For our purpose, we need a "digital" version of the uniqueness theorem to derive Equations (2)–(4). For this we define N_{psd} as the "perimetric sampling density" to be the total number of data points on the perimeter over the length of the perimeter in wavelength units. This parameter behaves much like the FD parameter $N_\lambda = \lambda/\Delta$, the sampling density of Equation (52) of Ref. [1]. We can say that when $N_{psd} > 2$, all the traveling waves within the surface $\mathbf{S}$ are captured by this set of discrete points on the perimeter of the area $\mathbf{S}$. When all sampled points on contours $C1$ or $C2$ are applied we can compute N_{psd} without any ambiguity. LFE-5+ and LFE-5X, however, use only half the data points on $C1$, therefore their contours are no longer a square. Instead, a circle with a radius of Δ is more appropriate for the perimeter of LFE-5+ and similarly, a circle of a radius $\sqrt{2}\Delta$ for LFE-5X. Thus, we

have:

$$N_{psd} = \begin{cases} 4\lambda/2\pi\Delta = \frac{4}{V} = \frac{2}{\pi}N_\lambda, \quad \text{(LFE-5+)} \\ 4\lambda/2\sqrt{2}\pi\Delta = \frac{2\sqrt{2}}{V} = \frac{\sqrt{2}}{\pi}N_\lambda, \quad \text{(LFE-5X)} \\ 8\lambda/8\Delta = \frac{2\pi}{V} = N_\lambda, \quad \text{(LFE-9)} \\ 16\lambda/16\Delta = \frac{2\pi}{V} = N_\lambda. \quad \text{(LFE-17)} \end{cases} \tag{5}$$

It is interesting to note that we may derive LFE-17 equation including the reconstruction formulae, following similar procedures for obtaining LFE-9. We hope that by allowing for a finer angular resolution (for a given local field) through the use of more points, it may help us to further lower the numerical dispersion errors. A quick verification of Equation (5) shows that both LFE-9 and LFE-17 have a same value of $N_{psd} = N_\lambda$. We anticipate that the local and global errors for LEF-17 are approximately the same as in LFE-9. However, the main disadvantage of the LFE-17 based FD-FD method is that the FD stencil is no longer compact and the additional effort required for solving the linear equation nullifies the small gain in accuracy.

3.3. Discrete Fourier Transform (DFT)

In the theory of connected local field, the procedure for obtaining local field expansion coefficients of any given patch is closely related to the algorithm of discrete Fourier transform. In fact, the local Fourier-Bessel coefficients are computed in the same way as the discrete Fourier transform [13–15] is applied to points on the perimeter. This is particularly true for both the LFE-5+ and LFE-5X formulations, because the data points are all on a circle centered at u_c and they are equally spaced as required by the DFT. For LFE-9, the points on the square do not lie on the same circle, therefore, direct application of the DFT to the eight sampled points does not produce the LFE-9 coefficients. However, $\Delta\phi_1$, the angular spacing between adjacent points on the $C1$ contour remains equal. This allows us to construct the LFE-9 coefficients as a linear combination of LFE-5+ DFT and LFE-5X DFT. We will further examine the details in Section 4.2. For data points on the $C2$ contour, the angular spacing $\Delta\phi_2$ is not a constant. Hence, the Fourier-Bessel coefficients of LFE-17 can not be obtained by directly applying the DFT.

4. CLOSED-FORM LOCAL ERROR ANALYSIS

In Ref. [1] we present numerical dispersion analysis for LFE-5 and LFE-9 formulation. In this section, we provide a closed-form, first-order error analysis for the method of connected local fields. In a source-free

linear homogeneous medium, the 2-D EM field can be expanded as the following infinite Fourier-Bessel series:

$$u(\rho,\phi) = a_0 J_0(k\rho) + \sum_{n=1}^{\infty} J_n(k\rho)(a_n \cos n\phi + b_n \sin n\phi), \tag{6}$$

with

$$\begin{aligned} a_0 &= \frac{1}{2\pi J_0(k\rho)} \int_0^{2\pi} u(\rho,\phi) d\phi, \\ a_n &= \frac{1}{\pi J_n(k\rho)} \int_0^{2\pi} u(\rho,\phi) \cos n\phi d\phi, \quad n \geq 1 \\ b_n &= \frac{1}{\pi J_n(k\rho)} \int_0^{2\pi} u(\rho,\phi) \sin n\phi d\phi. \quad n \geq 1 \end{aligned} \tag{7}$$

4.1. Local LFE-5 Errors

By choosing $\rho = \Delta$, we evaluate u_c and the four side points u_r, u_u, u_l, u_d with Equation (6). We have:

$$\begin{aligned} u_c &= a_0, \quad u_r = \sum_{n=0}^{\infty} a_n J_n(V), \\ u_l &= \sum_{n=0}^{\infty} (-1)^n a_n J_n(V), \\ u_u &= \sum_{m=0}^{\infty} (-1)^m a_{2m} J_{2m}(V) + \sum_{m=0}^{\infty} (-1)^m b_{2m+1} J_{2m+1}(V), \\ u_d &= \sum_{m=0}^{\infty} (-1)^m a_{2m} J_{2m}(V) - \sum_{m=0}^{\infty} (-1)^m b_{2m+1} J_{2m+1}(V). \end{aligned} \tag{8}$$

We then sum up these four side points which should be denoted as $u_\Sigma^+ = u_r + u_u + u_l + u_d$, and the result is given by:

$$\begin{aligned} u_\Sigma^+ &= 4a_0 J_0(V) + 4 \sum_{m=1}^{\infty} a_{4m} J_{4m}(V), \\ u_c = a_0 &= \frac{1}{4J_0(V)} (u_\Sigma^+ + O_{5+}). \end{aligned} \tag{9}$$

The second term in Equation (9) $O_{5+}(= -4 \sum_{m=1}^{\infty} a_{4m} J_{4m}(V))$ can be thought of as the high frequency aliasing signal to u_c due to inadequate

sampling. It is interesting to note that even though we only have four data points to match the lowest four Fourier coefficients a_0, a_1, a_2 and b_1, the leading term of O_{5+} is $a_4 J_4(V)$. To simplify this leading term we apply the following small argument Taylor's expansion of the Bessel function [16] :

$$J_m(z) = \sum_{k=0}^{\infty} \frac{(-1)^k}{\Gamma(m+k+1)k!} \left(\frac{z}{2}\right)^{2k+m} \approx \frac{1}{m!} \left(\frac{z}{2}\right)^m. \tag{10}$$

The local error for approximating u_c by LFE-5+ equation is denoted by E_{5+}. We then have:

$$E_{5+} \stackrel{\Delta}{=} u_c - \frac{u_\Sigma^+}{4J_0(V)} \approx -a_4 J_4(V) \approx \frac{-a_4}{384} V^4. \tag{11}$$

To derive the local truncation error for the LFE-5X equation we evaluate Equation (6) at all four corner points and, after summing up the result ($u_\Sigma^{\mathrm{x}} = u_{ne} + u_{nw} + u_{se} + u_{sw}$), we have:

$$\begin{aligned} u_\Sigma^{\mathrm{x}} &= 4a_0 J_0(\sqrt{2}V) + 4\sum_{m=1}^{\infty} (-1)^m a_{4m} J_{4m}(\sqrt{2}V), \\ u_c = a_0 &= \frac{1}{4J_0(\sqrt{2}V)} (u_\Sigma^{\mathrm{x}} + O_{5X}). \end{aligned} \tag{12}$$

Here O_{5X} represents the sum of all high-order aliasing terms ($= -4\sum_{m=1}^{\infty} (-1)^m a_{4m} J_{4m}(\sqrt{2}V)$) in u_c. Finally, the local truncation error for the LFE-5X equation is given by:

$$E_{5X} \stackrel{\Delta}{=} u_c - \frac{u_\Sigma^{\mathrm{x}}}{4J_0(\sqrt{2}V)} \approx \frac{a_4}{J_0(\sqrt{2}V)} J_4(\sqrt{2}V) \approx \frac{a_4}{96} V^4. \tag{13}$$

The local truncation errors of the two LFE-5 equations are proportional to the fourth power of the normalized frequency V and the unknown fourth-order local Fourier-Bessel coefficient a_4. Comparing Equations (13) with (11), the local truncation errors of the two LFE-5X is four times that of LFE-5+.

4.2. An Alternate Derivation for the LFE-9 Equation

We may further reduce the local error by combing the two LFE-5 equations with specific coefficients for Equations (2) and (3) so that the leading a_4 term in the final result is completely eliminated. From Equations (11), (13), we see that the following weighting factors lead to

LFE-9 coefficients: (see also Equation (22) of Ref. [1] for the algebraic derivation):

$$\begin{aligned} &J_4(\sqrt{2}V)u_{\Sigma}^{+} + J_4(V)u_{\Sigma}^{\mathrm{x}} = 4(W_9)u_c + O_9, \\ &W_9 = J_4(\sqrt{2}V)J_0(V) + J_4(V)J_0(\sqrt{2}V), \\ &O_9 = 4\sum_{m=2}^{\infty} a_{4m}\left[J_4(\sqrt{2}V)J_{4m}(V) + (-1)^m J_4(V)J_{4m}(\sqrt{2}V)\right]. \end{aligned} \tag{14}$$

4.3. Local LFE-9 Errors

Thus, from the leading term of O_9, the leading local error E_9 for LFE-9 formulation is given by:

$$\begin{aligned} E_9 &= \frac{a_8\left[J_4(\sqrt{2}V)J_8(V) - J_4(V)J_8(\sqrt{2}V)\right]}{J_4(\sqrt{2}V)J_0(V) + J_4(V)J_0(\sqrt{2}V)}, \\ &\approx -a_8\left[\frac{4}{5}J_8(V) - \frac{1}{5}J_8(\sqrt{2}V)\right] \approx \frac{1}{8!}\frac{3}{320}a_8V^8 = \left(\frac{a_8}{4300800}\right)V^8 \end{aligned} \tag{15}$$

The local errors of the LFE-9 equations are proportional to the 8th power of the normalized frequency V and the unknown 8th local Fourier-Bessel coefficient a_8.

If we compare the order of error between E_9 and E_{5+}, assuming $a_8 \approx a_4$, we see that when $V < 1$, the local truncation error E_{5+} is at least ten thousand times larger than E_9. Even at the lowest sampling rate, $V = \pi$, the LFE-5 local error is still about one hundred times greater than that of the LFE-9.

5. NORMALIZED DISCRETE 2-D HELMHOLTZ OPERATOR

Now we are in a good position to derive the normalized discrete 2-D Helmholtz operator based on the LFE formulation. The homogeneous, source-free, 2-D Helmholtz operator is given below:

$$Lu(z,x) = 0, \quad L = \nabla_t^2 + k^2. \tag{16}$$

Let $\hat{L}$ be the normalized, discrete 2-D Helmholtz operator of L. The general symmetric form for the discrete operator involving all nine points in Figure 1 can be written as (see Equation (9), Ref. [1]):

$$\hat{L}u_c = 0, \quad \Rightarrow \quad A_c u_c + A_+ u_{\Sigma}^{+} + A_{\mathrm{x}} u_{\Sigma}^{\mathrm{x}} = 0. \tag{17}$$

Here the coefficients A_c, A_+, A_{x} are functions of k and spatial discretization size Δ.

5.1. Normalized Discrete FD Helmholtz Operators

Next we list $\hat{L}_{\text{FD2-5+}}$ and $\hat{L}_{\text{FD2-5X}}$, the standard 2nd-order accurate FD approximation of the continuous 2-D Helmholtz operator below:

$$\left(\frac{-4}{\Delta^2}+k^2\right)\cdot u_c+\frac{1}{\Delta^2}\cdot u_\Sigma^+ + 0\cdot u_\Sigma^{\text{x}}=0, \quad \left(\hat{L}_{\text{FD2-5+}}\right), \tag{18}$$

and

$$\left(\frac{-2}{\Delta^2}+k^2\right)\cdot u_c+0\cdot u_\Sigma^+ + \frac{1}{2\Delta^2}\cdot u_\Sigma^{\text{x}}=0. \quad \left(\hat{L}_{\text{FD2-5X}}\right). \tag{19}$$

Note that any normalized (sum of weighting factors equals to 1) linear combination of Equations (18) and (19) is also a valid 2nd-order accurate discrete Helmholtz operator. Further analysis shows that by eliminating the lowest-order cross partial derivative term in the truncation error (Ref. [6], 218–220), we may derive the normalized, 2nd-order accurate, discrete Helmholtz operator $\hat{L}_{\text{FD2-9}}$ (Equation (10), Ref. [1]) as:

$$\begin{aligned}\hat{L}_{\text{FD2-9}} &= \frac{2}{3}\cdot\hat{L}_{\text{FD2-5+}}+\frac{1}{3}\cdot\hat{L}_{\text{FD2-5X}},\\ &= \left(-\frac{10}{3}\frac{1}{\Delta^2}+k^2\right)\cdot u_c+\frac{2}{3}\cdot\frac{u_\Sigma^+}{\Delta^2}+\frac{1}{6}\cdot\frac{u_\Sigma^{\text{x}}}{\Delta^2}.\end{aligned} \tag{20}$$

For comparison, the expression for the normalized, 6th-order accurate, discrete Helmholtz operator $\hat{L}_{\text{FD6-9}}$ is given by (see Equation (10), Ref. [1]):

$$\begin{aligned}\hat{L}_{\text{FD6-9}} &= A_c^{\text{FD6-9}}\cdot u_c + A_+^{\text{FD6-9}}\cdot u_\Sigma^+ + A_X^{\text{FD6-9}}\cdot u_\Sigma^{\text{x}}.\\ A_c^{\text{FD6-9}} &= -\frac{10}{3}\frac{1}{\Delta^2}+\left(\frac{46}{45}-\frac{k^2\Delta^2}{12}+\frac{k^4\Delta^4}{360}\right)k^2,\\ A_+^{\text{FD6-9}} &= \frac{2}{3}\frac{1}{\Delta^2}\left(1-\frac{k^2\Delta^2}{60}\right),\\ A_X^{\text{FD6-9}} &= \frac{1}{6}\frac{1}{\Delta^2}\left(1+\frac{k^2\Delta^2}{30}\right).\end{aligned} \tag{21}$$

This novel compact 9-point FD-FD stencil [17] provides fairly accurate results with low sampling densities of three to four points per wavelength.

5.2. Normalized Discrete LFE Helmholtz Operators

The Taylor series for the Bessel function $J_m(z)$ and in particular $J_0(z)$, are given below:

$$\begin{aligned} J_m(z) &= \sum_{k=0}^{\infty} \frac{(-1)^k}{(m+k)!k!} \left(\frac{z}{2}\right)^{2k+m}, \quad m = 0, 1, 2, \ldots \\ J_0(z) &= 1 + \sum_{k=1}^{\infty} \frac{(-1)^k}{(k!)^2} \left(\frac{z}{2}\right)^{2k} \approx 1 - \frac{z^2}{4}. \end{aligned} \tag{22}$$

To find $\hat{L}_{\text{LFE-5+}}$ and $\hat{L}_{\text{LFE-5X}}$, the normalized, discrete 2-D Helmholtz operators based on LFE formulation, we expand $J_0(z)$ and $J_0(\sqrt{2}z)$ of Equations (2), (3) by the first two terms of its Taylor series and compare the results with Equations (18), (19). We conclude that:

$$\hat{L}_{\text{LFE-5+}} = -\frac{4J_0(k\Delta)}{\Delta^2} \cdot u_c + \frac{1}{\Delta^2} \cdot u_\Sigma^+ + 0 \cdot u_\Sigma^{\text{x}}, \tag{23}$$

and

$$\hat{L}_{\text{LFE-5X}} = -\frac{4J_0(\sqrt{2}k\Delta)}{2\Delta^2} \cdot u_c + 0 \cdot u_\Sigma^+ + \frac{1}{2\Delta^2} \cdot u_\Sigma^{\text{x}}. \tag{24}$$

Following the argument of Section 4.2, we derive $\hat{L}_{\text{LFE-9}}$ as a linear combination of $\hat{L}_{\text{LFE-5+}}$ and $\hat{L}_{\text{LFE-5X}}$ operators. The resulting u_Σ^+ and u_Σ^x coefficients must be proportional to the corresponding coefficients in Equation (14) and the two weighting coefficients must also sum up to one. By inspection, we see that the following expressions meet these two conditions, and thereby represent the normalized, LFE-9 based discrete 2-D Helmholtz operator.

$$\begin{aligned} \hat{L}_{\text{LFE-9}} =& \frac{1}{J_4(\sqrt{2}V) + 2J_4(V)} \\ & \left(J_4(\sqrt{2}V) \cdot \hat{L}_{\text{LFE-5+}} + 2J_4(V) \cdot \hat{L}_{\text{LFE-5X}}\right) \\ =& A_c^{\text{LFE-9}} \cdot u_c + A_+^{\text{LFE-9}} \cdot u_\Sigma^+ + A_X^{\text{LFE-9}} \cdot u_\Sigma^{\text{x}}. \quad (V = k\Delta) \\ A_c^{\text{LFE-9}} =& \frac{-4\left[J_0(V)J_4(\sqrt{2}V) + J_0(\sqrt{2}V)J_4(V)\right]}{\Delta^2\left[J_4(\sqrt{2}V) + 2J_4(V)\right]}, \\ A_+^{\text{LFE-9}} =& \frac{1}{\Delta^2} \frac{J_4(\sqrt{2}V)}{J_4(\sqrt{2}V) + 2J_4(V)}, \\ A_X^{\text{LFE-9}} =& \frac{1}{\Delta^2} \frac{J_4(V)}{J_4(\sqrt{2}V) + 2J_4(V)}. \end{aligned} \tag{25}$$

To check our derivation and to compare $\hat{L}_{\text{LFE-9}}$ with $\hat{L}_{\text{FD6-9}}$ we expand all Bessel function arguments with Taylor series and maintain accuracy up to the fourth power of V, the normalized frequency. Thus, we have:

$$\begin{aligned} A_c^{\text{LFE-9}} &= -\frac{10}{3}\frac{1}{\Delta^2} + \left(\frac{46}{45} - \frac{307}{4320}V^2 + \frac{7}{1382400}V^4\right)\cdot k^2, \\ A_+^{\text{LFE-9}} &= \frac{2}{3}\frac{1}{\Delta^2}\left(1 - \frac{V^2}{60} - \frac{V^4}{2880}\right), \\ A_X^{\text{LFE-9}} &= \frac{1}{6}\frac{1}{\Delta^2}\left(1 + \frac{V^2}{30} + \frac{V^4}{1440}\right). \end{aligned} \tag{26}$$

We see that $A_+^{\text{FD6-9}}$ and $A_X^{\text{FD6-9}}$ agree with $A_+^{\text{LFE-9}}$ and $A_X^{\text{LFE-9}}$ exactly up to the second power of V, but the coefficient of $A_c^{\text{FD6-9}}$ differs slightly with $A_c^{\text{LFE-9}}$ in the second power of V. In fact, Equation (26) provides independent verification of the complex Equation (21) which was derived in a completely different way than our current approach.

6. CLOSED-FORM FIRST-ORDER GLOBAL ERROR ANALYSIS

The basis for local errors in Equations (11), (13), (15) stem from either point or line-source excitations or from the radiation field near a material discontinuity. When the fields are adequately sampled under the condition $N_\lambda > 2 (V < \pi)$, the higher-order Fourier-Bessel terms of Equation (6) contain evanescent waves that stay local near the sources. However, the global errors are from propagating waves in the solution, and this type of error does not decay far away from excitation sources. They must be analyzed against propagating plane waves in all possible directions. We introduced the plane wave dispersion analysis in Ref. [1] where we numerically examined phase dispersion errors. To obtain a closed-form expression for the global errors in the LFE-5X and LFE-9 formulation, we turn to the method of first-order analysis, which will be explained in detail in Section 6.2.

6.1. Summary of Dispersion Characteristics

We first list the exact dispersion equation for LFE-5 case in the following (Equation (41), Ref. [1]):

$$2J_0(V) = \cos(B\cos\theta) + \cos(B\sin\theta), \quad B = \kappa\Delta. \tag{27}$$

This nonlinear equation gives the exact relation between κ and $\mathbf{k}$, the numerical and the analytical wavenumber of the plane wave propagating in an infinite homogeneous medium. In other words, the

numerical $\kappa(V,\theta)$ is an implicit function of $\mathbf{k}$ which is a function of the normalized frequency V and direction of propagation θ. The exact dispersion equation for LFE-9 case is given by (Ref. [1], Equation (42)):

$$\begin{aligned} & 2\left[J_0(\sqrt{2}V)\cdot J_4(V)+J_0(V)\cdot J_4(\sqrt{2}V)\right] \\ = \; & J_4(\sqrt{2}V)\cdot[\cos(B\cos\theta)+\cos(B\sin\theta)] \\ & +J_4(V)\cdot(\cos(\sqrt{2}B\cos(\theta-\pi/4))+\cos(\sqrt{2}B\sin(\theta-\pi/4))). \end{aligned} \tag{28}$$

6.2. First-order Analysis

For LFE-9, the relative difference between numerical and analytical normalized frequency B and V is minuscule. The first step in the first-order analysis is to express:

$$B = V(1+\varepsilon), \tag{29}$$

where $\varepsilon = \varepsilon(\omega,\Delta,\theta)$ is also regarded as a relative propagation constant error. In the spirit of the first-order analysis, we further assume that $\varepsilon \ll 1$ and terms including ε^2, ε^3 and other higher-order power(s) can be neglected. Based on this principle we published an approximation expression for $\varepsilon_{\text{LFE-9}}$ (Equation (55), Ref. [1]), but we omitted the derivation due to its complexity. Since B appears to be an argument inside the trigonometric functions on the right hand sides of Equations (27)–(28), in order to continue our analysis, we also need the following Jacobi-Anger Bessel function identities (361, 9.1.42–45 of Ref. [16]),

$$\begin{aligned} \cos(z\sin\theta) &= J_0(z)+2\sum_{m=1}^{\infty}[J_{2m}(z)\cos(2m\theta)], \\ \cos(z\cos\theta) &= J_0(z)+2\sum_{m=1}^{\infty}[(-1)^m J_{2m}(z)\cos(2m\theta)]. \end{aligned} \tag{30}$$

Substituting Equation (30) into Equation (27) and rearranging terms, we have:

$$J_0(V) = J_0(B)+2\sum_{m=1}^{\infty}[J_{4m}(B)\cos(4m\theta)] = 0. \tag{31}$$

Next, we expand the Bessel function $J_{4m}(B)$ with the Taylor expansion and then apply Equation (29) to the result. We have:

$$\begin{aligned} J_{4m}(B) &= \sum_{k=0}^{\infty} \frac{(-1)^k(1+\varepsilon)^{2k+4m}}{(4m+k)!k!}\left(\frac{V}{2}\right)^{2k+4m} \quad (B = V(1+\varepsilon)) \\ &\approx \sum_{k=0}^{\infty} \frac{(1+(2k+4m)\varepsilon)(-1)^k}{(4m+k)!k!}\left(\frac{V}{2}\right)^{2k+4m}, \\ &= J_{4m}(V) + \left(\frac{\varepsilon V}{2}\right)\sum_{k=0}^{\infty} \frac{(-1)^k(2k+4m)}{(4m+k)!k!}\left(\frac{V}{2}\right)^{2k+4m-1}, \\ &= J_{4m}(V) + (\varepsilon V)\frac{d}{dV}\sum_{k=0}^{\infty} \frac{(-1)^k}{(4m+k)!k!}\left(\frac{V}{2}\right)^{2k+4m}, \\ &= J_{4m}(V) + \varepsilon\left(V\frac{dJ_{4m}(V)}{dV}\right). \quad m = 0, 1, 2, \ldots \end{aligned} \tag{32}$$

Equation (31) is obtained by using the first-order approximation to the perturbation variable ε, where we delete terms containing higher power(s) of ε, and keep only the linear terms. Let $m = 0$ in Equation (32), we have:

$$\begin{aligned} J_0(B) &= J_0(V) + \varepsilon \cdot \left(V\frac{dJ_0(V)}{dV}\right), \\ &= J_0(V) - \varepsilon \cdot VJ_1(V). \end{aligned} \tag{33}$$

6.3. First-order Dispersion Error for LFE-5

Substituting Equation (32)–(33) into Equation (31), and then solve for ε, we may list $\varepsilon_{\text{LFE-5}}$ as follows:

$$\varepsilon_{\text{LFE-5}} = \frac{2\sum\limits_{m=1}^{\infty} J_{4m}(V)\cos(4m\theta)}{V\left\{J_1(V) - 2\sum\limits_{m=1}^{\infty}\left[\frac{dJ_{4m}(V)}{dV}\cos(4m\theta)\right]\right\}}. \tag{34}$$

Further simplification is possible by Taylor expansion of the Bessel functions. A useful expression with two Fourier terms in the numerator and one term in the denominator gives:

$$\varepsilon_{\text{LFE-5}} = \frac{V^2\left(1-\frac{V^2}{20}+\frac{V^4}{960}\right)\cos 4\theta + \frac{3}{7!16}V^6\left(1-\frac{V^2}{18}+\frac{V^4}{576}\right)\cos 8\theta}{96\left[1-\left(\frac{12+4\cos 4\theta}{96}\right)V^2+\left(\frac{5+11\cos 4\theta}{960}\right)V^4\right]} \tag{35}$$

An immediate application of Equation (35) leads to an explanation of the superior performance of LFE-5 at specific directions (see Figure 10, Ref. [1]) when $\cos 4\theta = 0$. We have:

$$\varepsilon_{\text{LFE-5}}\left(\theta = \frac{(2n-1)\,\pi}{8}\right) = \left[\frac{-0.387\left(1-\frac{V^2}{18}+\frac{V^4}{576}\right)}{1-\frac{V^2}{8}+\frac{V^4}{192}}\right]\left(\frac{V}{10}\right)^6. \quad n = 1, 2, 3\ldots \tag{36}$$

6.4. First-order Dispersion Error for LFE-9

Comparing Equation (27) with Equation (31), we have

$$\cos(B\cos\theta) + \cos(B\sin\theta) = 2J_0(B) + 4\sum_{m=1}^{\infty}[J_{4m}(B)\cos(4m\theta)]. \tag{37}$$

Similarly, we have

$$\begin{aligned} &\cos\left(\sqrt{2}B\cos(\theta-\pi/4)\right) + \cos\left(\sqrt{2}B\sin(\theta-\pi/4)\right) \\ =\ & 2J_0(\sqrt{2}B) + 4\sum_{m=1}^{\infty}\left[(-1)^m J_{4m}(\sqrt{2}B)\cos(4m\theta)\right] = 0. \end{aligned} \tag{38}$$

Substituting Equations (37)–(38) into Equation (28) yields:

$$\begin{aligned} &2\left[J_0(\sqrt{2}V)\cdot J_4(V) + J_0(V)\cdot J_4(\sqrt{2}V)\right] \\ =\ & J_4(\sqrt{2}V)\cdot\left[2J_0(B) + 4\sum_{m=1}^{\infty}[J_{4m}(B)\cos(4m\theta)]\right] \\ & + J_4(V)\cdot\left(2J_0(\sqrt{2}B) + 4\sum_{m=1}^{\infty}\left[(-1)^m J_{4m}(\sqrt{2}B)\cos(4m\theta)\right]\right). \end{aligned} \tag{39}$$

Next, applying Equations (32) to (39), we may then solve for $\varepsilon_{\text{LFE-9}}$ and the result is:

$$\begin{aligned} \varepsilon_{\text{LFE-9}} &= \frac{\sum_{m=1}^{\infty}\left[J_4(\sqrt{2}V)J_{4m}(V) + (-1)^m J_4(V)J_{4m}(\sqrt{2}V)\right]\cos(4m\theta)}{V(D_1 - D_2)}, \\ D_1 &= \frac{1}{2}J_1(V)J_4(\sqrt{2}V) + \frac{1}{\sqrt{2}}J_1(\sqrt{2}V)J_4(V), \\ D_2 &- \sum_{m=1}^{\infty}\left[J_4(\sqrt{2}V)\frac{dJ_{4m}(V)}{dV} + (-1)^m J_4(V)\frac{dJ_{4m}(\sqrt{2}V)}{dV}\right]\cos(4m\theta). \end{aligned} \tag{40}$$

Like the previous case, further simplification is possible by keeping just first two terms in the Fourier series as the numerator and using just the first term in the denominator. We have:

$$\begin{aligned}\varepsilon_{\text{LFE-9}} &= \frac{N_1\cos 8\theta + N_2\cos 12\theta}{V\cdot(D_1 - D_3\cos 4\theta)}.\\ N_1 &= J_4(\sqrt{2}V)J_8(V) + J_4(V)J_8(\sqrt{2}V),\\ N_2 &= J_4(\sqrt{2}V)J_{12}(V) - J_4(V)J_{12}(\sqrt{2}V),\\ D_3 &= J_4(\sqrt{2}V)\frac{dJ_4(V)}{dV} - J_4(V)\frac{dJ_4(\sqrt{2}V)}{dV}\end{aligned} \tag{41}$$

To derive Equation (55) of Ref. [1] from Equation (41), we apply the Taylor expansion to the Bessel functions and the following Bessel identity:

$$\frac{dJ_m(V)}{dV} = \frac{m}{V}J_m(V) - J_{m+1}(V). \tag{42}$$

The final result is given below:

$$\begin{aligned}\varepsilon_{\text{LFE-9}} &= \left(\frac{N_3\cos 8\theta - N_4\cos 12\theta}{D_4}\right)\left(\frac{V}{10}\right)^6\\ N_3 &= 1.29\left(1 - \frac{11}{100}V^2 + \frac{1}{225}V^4\right),\\ N_4 &= 0.2\left(\frac{V}{10}\right)^4\left(1 - \frac{337}{3900}V^2 + \frac{217}{62400}V^4\right),\\ D_4 &= 1 - \frac{1}{4}V^2 + \left(\frac{33-\cos 4\theta}{1440}\right)V^4.\end{aligned} \tag{43}$$

We added an additional term (other than Equation (55) of Ref. [1]) to Equation (43) to the numerator so that we can see that at the special angles $\theta = \pi/16$, $3\pi/16$ and etc., the relative dispersion error of LFE-9 is even several orders higher than V^6.

$$\varepsilon_{\text{LFE-9}}\left(\theta = \frac{(2n-1)\pi}{16}\right) \approx \pm 0.14\left(\frac{V}{10}\right)^{10}. \quad n = 1, 2, 3\ldots \tag{44}$$

7. NUMERICAL VERIFICATION

7.1. Numerical Verification of the First-order Error Analysis

In deriving the analytical expression for the LFE global error we made an assumption that $\varepsilon \ll 1$ in Equation (29). Under said conditions, the first-order analysis allows us to drop all terms containing higher

power(s) of ε, and in the end, leads us to Equations (34)–(36) and (40)–(44). In Ref. [1] we conducted detail numerical calculations of B with the exact dispersion relation (Equations (27)–(28)) and found that $\varepsilon_{\text{LFE-9}} \ll 1$ for all $\theta \in [0, 2\pi]$ and all $V \in [0, \pi]$. But for LFE-5, the relative B-K differences are much larger, thus $\varepsilon_{\text{LFE-5}} \ll 1$ is not always satisfied. In fact, for some directions, we are unable to find a real solution for $B_{\text{LFE-5}}$ when V is close to π.

As a result, we expect the analytical expression for $B_{\text{LFE-9}}$ to be fairly accurate through out the valid ranges of V and θ. This is also true for the analytical expression for $B_{\text{LFE-5}}$ when $V \ll 1$. Numerical evidence shows that, for the maximum difference between numerically computed $B^N_{\text{LFE-9}}$ and the analytical evaluated $B^A_{\text{LFE-9}}$, computed by applying Equation (29) to Equation (40), are well under a few percents even for V as large as π, the maximum value.

7.2. Numerical Verification of CLF Computation of the Two-Dimensional Green's Function

In this section we will examine the two-D LFE-5 and LFE-9 formulae by a direct comparison with the exact analytical solution of the free space Green's function. We know that the two-D Green's function is the solution of the following Helmholtz equation due to a line source located in the origin:

$$(\nabla_t^2 + k_0^2)G(x, z) = -\delta(x)\delta(z). \tag{45}$$

The analytic closed-form solution is given in terms of the Hankel function of the second kind [10] as follows:

$$G(\rho) = -\frac{j}{4}H_0^{(2)}(k_0\rho), \quad \rho = \sqrt{x^2 + z^2} \tag{46}$$

As shown in Figure 3, the computational domain is an $L_x \times L_z$ rectangle in the first quadrant bound by two solid green lines and two dotted red lines. On the green lines the Neumann's boundary condition (NBC) is applied whereas on the red lines the transparent boundary condition (TBC) is implemented. For points on the NBC lines, LFE equations are modified by reflecting the exterior node back onto its mirrored, interior node [Equations (5)–(6). Ref. 18]. For points on the TBC lines we use the following expression for relating the points outside the computing region to their nearest corresponding TBC point:

$$u_{ext} = u_{tbc} \cdot \left[\frac{H_0^{(2)}(k\rho_{ext})}{H_0^{(2)}(k\rho_{tbc})} \right], \tag{47}$$

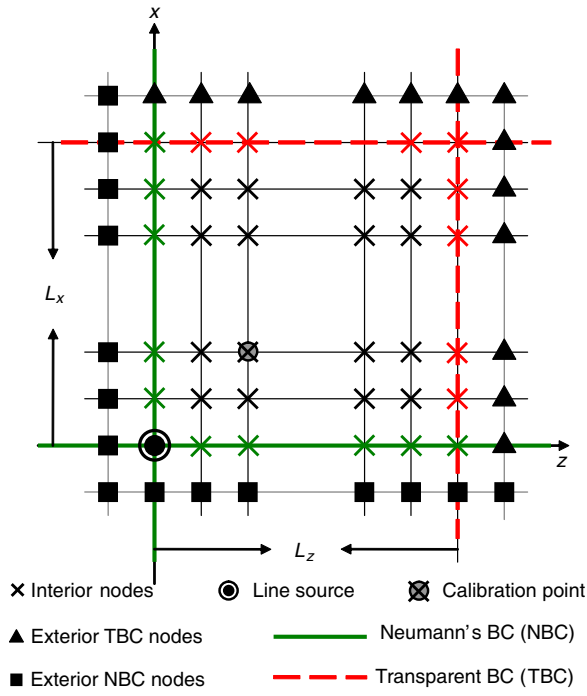

Figure 3. The grid layout for computing two-dimensional Green's function. The line source is located at the origin. For this unbound problem, the computational domain, which is an $L_x \times L_z$ rectangle, is bound by two solid green lines and two dotted ret lines. The green lines represent the Neumann's boundary condition (NBC) while the red lines represent transparent boundary conditions (TBC). We apply the LFE equation to the interior nodes as marked by black crosses, whereas the modified LFE equation is applied to the green and red crosses on the border lines.

where ρ_{ext} is the distance of the exterior point to the origin and ρ_{tbc} is the distance of the corresponding TBC point to the origin. The ratio term in Equation (47) is the effective impedance for the outgoing wave at the said TBC point.

To compensate for the strength difference between the analytical and the numerical source terms, both Green's functions are normalized so that the analytic $G_a(x,z)$ and numerical $G_n(x,z)$ are equal at the calibration point (see legend in Figure 3). The normalization procedure is carried out by the following equation:

$$\tilde{G}_n(x_i,z_j) = \frac{G_n(x_i,z_j)}{G_n(k_\lambda\Delta,k_\lambda\Delta)}, \quad \tilde{G}_a(x,z) = \frac{G_a(x,z)}{G_a(k_\lambda\Delta,k_\lambda\Delta)}. \tag{48}$$

Here k_λ, a rounded integer of λ/N_λ, represents the nearest integer number of sampling points per wavelength. We then compute the relative differences between these two calibrated data sets. To start with, the relative amplitude error $e^a_{i,j}$ at point (x_i, z_j) is defined as:

$$e^a_{i,j} \triangleq \frac{\left|\tilde{G}_n(i,j)\right| - \left|\tilde{G}_a(x_i, z_j)\right|}{\left|\tilde{G}_a(x_i, z_j)\right|}. \tag{49}$$

For dispersion error we need to examine the relative amplitude and the phase error $e^p_{i,j}$, which is computed as such:

$$e^p_{i,j} \triangleq \frac{\left|\tilde{G}_n(x_i, z_j) - \tilde{G}_a(x_i, z_j)\right|}{\left|\tilde{G}_a(x_i, z_j)\right|}. \tag{50}$$

The overall relative error can be best summarized by computing the root mean squares (RMS) of each local error using the following

Table 1. Comparison of relative amplitude RMS errors of various frequency-domain methods under a range of sampling densities.

Relative difference (amplitude only)				
N_λ	FD2-5	FD2-9	LFE-5	LFE-9
3	N.A*.	N.A	N.A	0.024148
4	N.A	N.A	N.A	0.005219
5	N.A	N.A	0.11395	0.001829
6	0.10331	0.03542	0.07991	0.000815
7	0.04641	0.02316	0.05629	0.000421
8	0.04247	0.01380	0.04133	0.000240
9	0.03996	0.01206	0.03166	0.000147
10	0.03378	0.01089	0.02512	0.000095
12	0.02169	0.00668	0.01698	0.000045
15	0.01186	0.00348	0.01063	0.000018
20	0.00579	0.00204	0.00590	0.000006
25	0.00350	0.00140	0.00376	0.000002
30	0.00236	0.00101	0.00260	0.000001

*N.A. stands for not applicable.

expression:

$$E_{RMS}^{a,p} \triangleq \sqrt{\frac{1}{L_x L_z N_\lambda^2 - k_\lambda^2} \sum_{i,j} \left(e_{i,j}^{a,p}\right)^2}, \; \lambda < x_i \leq L_x, \; \lambda < z_j \leq L_z. \quad (51)$$

Note that to reduce the near field error caused by the highly singular delta function, we exclude points that are very close to the line source. In Table 1 we tabulate the RMS relative amplitude errors of two-dimensional calculation of the Green's function using FD2-5, FD2-9, LFE-5 and LFE-9 stencils. We also assume that $L_x = L_z = 12\lambda$. To study the numerical convergent properties of these various frequency-domain formulations we extend the linear sampling density N_λ from three to thirty points per wavelength. There are a total of $144N_\lambda^2$ unknowns used in the linear equation. We use a modified Thomas method [18, 19] for a direct LU factorization of the tri-diagonal block linear equation. At $N_\lambda = 30$ a maximum of one hundred and thirty thousand unknowns were present, and it took about ninety seconds of CPU time on a PC using Matlab.

We see from Table 1 that the traditional FD-FD methods requires an $N_\lambda > 15$ to keep the RMS amplitude error under one percent. Still,

Table 2. Comparison of relative 2-D Green's function amplitude and phase RMS errors of various frequency-domain methods.

Relative difference (amplitude and phase)				
N_λ	FD2-5	FD2-9	LFE-5	LFE-9
3	N.A*.	N.A.	N.A.	0.035928
4	N.A	N.A	N.A	0.008137
5	N.A	N.A	0.860718	0.002926
6	N.A	N.A	0.594987	0.001322
7	1.23155	1.57234	0.431682	0.000687
8	0.98675	1.33579	0.326708	0.000393
9	0.79046	1.10529	0.255753	0.000242
10	0.63961	0.91189	0.205660	0.000157
12	0.43975	0.63951	0.141368	0.000074
15	0.27868	0.40981	0.089666	0.000030
20	0.15577	0.23032	0.050063	0.000009
25	0.09946	0.14729	0.031924	0.000004
30	0.06899	0.10223	0.022124	0.000002

*N.A. stands for not applicable.

this is quite acceptable considering that the simulation domain is over one hundred square wavelengths. However, with the LFE-9 stencil the same level of accuracy is achieved with an N_λ slightly greater than 3. Furthermore, the convergent rate of LFE-9 is also faster than those traditional FD-FD methods. The advantage of the local field method is best demonstrated when we compare the RMS amplitude and phase error as listed in Table 2. For this tighter error criterion, the traditional FD-FD methods perform poorly. We see that even at $N_\lambda = 30$, which is quite high for running practical FD-FD simulations, both the FD2-5 and the FD2-9 can not maintain the under one percent overall phase error. It is interesting to note that the LFE-9 does not deteriorate as much under the tougher measure of error.

Some of the entries in Tables 1 and 2 are marked with "N.A" because of the excessive errors in the computed results due to inadequate sampling density. In fact, the phase errors are accumulating as the EM fields propagate away from the source at the origin. Near the edge of the computational domain the phase errors exceed multiple of πs.

8. CONCLUSIONS

The recently developed CLF theory shows a promising potential in its ability to obtain, highly accurate semi-numerical, solutions of the Helmholtz equation in a general inhomogeneous medium. The primary result is the new nine-point stencil based on local Fourier-Bessel expansion for the 2-D Helmholtz equation in a homogeneous medium. Early numerical evidence shows that the method of CLF outperforms, by a factor of ten, other high-order FD-FD methods due to LFE-9's super-linear B-K relation. As a result, tremendous savings in computer resources are made possible with this new numerical formulation.

In this paper, we lay down the theoretical foundation for CLF. We show that the core theory is the result of applying the uniqueness theorem together with the theory of discrete Fourier transform. We derive the normalized discrete 2-D Helmholtz operators for LFE-5 and LFE-9 stencils. We also present a theoretical analysis of the local truncation errors as a function of the normalized frequency. And for the global error due to inadequate spatial and directional sampling of propagating plane waves, we provide highly accurate, closed-form expression of normalized numerical frequency for the LFE-9 formulation. We also conduct a thorough numerical LFE simulation of two-dimensional Green's function. The results compare well with the exact analytical solution. The analytical error analysis on the

local and global CLF errors helps us to better choose the computational parameter N_λ in CLF applications. At the end, we have a much better, more intuitive understanding of how CLF works.

ACKNOWLEDGMENT

We are grateful for the support of the National Science Council of the Republic of China under the contracts NSC98-2221-E110-012. This work is also supported by the Ministry of Education, Taiwan, R.O.C., under the Aim-for-the-Top University Plan.

REFERENCES

1. Chang, H.-W. and S.-Y. Mu, "Semi-analytical solutions of 2-D Homogeneous Helmholtz equation by the method of connected local fields," *Progress In Electromagnetics Research*, Vol. 109, 399–424, 2010.
2. Chang, H.-W. and S.-Y. Mu, "Novel nine-point FD coefficients for the two-dimensional Helmholtz equation," *Cross Strait Tri-Regional Radio Science and Wireless Technology Conference*, Hanan, China, 2010.
3. Chang, H.-W. and S.-Y. Mu, "Frequency dependent FD-like coefficients for 2-D Helmholtz equation derived from local Fourier-Bessel series," *The 6th International Conference on Photonics and Applications, ICPA-6 2010*, HaNoi, Vietnam, 2010.
4. Chang, H.-W. and S.-Y. Mu, "Dispersion analysis of Fourier-Bessel series derived FD coefficients for two-dimensional Helmholtz equation," *The 6th International Conference on Photonics and Applications, ICPA-6 2010*, HaNoi, Vietnam, 2010.
5. Kuzu, L., V. Demir, A. Z. Elsherbeni, and E. Arvas, "Electromagnetic scattering from arbitrarily shaped chiral objects using the finite difference frequency domain method," *Progress In Electromagnetics Research*, Vol. 67, 1–24, 2007.
6. Jung, B. H. and T. K. Sarkar, "Solving time domain Helmholtz wave equation with MOD-FDM," *Progress In Electromagnetics Research*, Vol. 79, 339–352, 2008.
7. Chang, H.-W., W.-C. Cheng, and S.-M. Lu, "Layer-mode transparent boundary condition for the hybrid FD-FD method," *Progress In Electromagnetics Research*, Vol. 94, 175–195, 2009.
8. Zheng, G., B.-Z. Wang, H. Li, X.-F. Liu, and S. Ding, "Analysis of finite periodic dielectric gratings by the finite-difference frequency-domain method with the sub-entire-domain basis functions and

wavelets," *Progress In Electromagnetics Research*, Vol. 99, 453–463, 2009.

9. Chang, H.-W. and Y.-H. Wu, "Analysis of perpendicular crossing dielectric waveguides with various typical index contrasts and intersection profiles," *Progress In Electromagnetics Research*, Vol. 108, 323–341, 2010.
10. Ishimaru, A., *Electromagnetic Propagation, Radiation, and Scattering*, Prentice Hall, Englewood Cliffs, N.J., 1991.
11. Zhou, X., "On independence, completeness of Maxwell's equations and uniqueness theorems in electromagnetics," *Progress In Electromagnetics Research*, Vol. 64, 117–134, 2006.
12. Zhou, X., "On uniqueness theorem of a vector function," *Progress In Electromagnetics Research*, Vol. 65, 93–102, 2006.
13. Semnani, A. and M. Kamyab, "Truncated cosine Fourier series expansion method for solving 2-D inverse scattering problems," *Progress In Electromagnetics Research*, Vol. 81, 73–97, 2008.
14. Zhao, Y. W., M. Zhang, and H. Chen, "An efficient ocean SAR RAW signal simulation by employing fast Fourier transform," *Journal of Electromagnetic Waves and Applications*, Vol. 24, No. 16, 2273–2284, 2010.
15. Zhu, C.-H., Q. H. Liu, Y. Shen, and L. Liu, "A high accuracy conformal method for evaluating the discontinuous Fourier transform," *Progress In Electromagnetics Research*, Vol. 109, 425–440, 2010.
16. Abramowitz, M. and I. A. Stegun, eds., *Handbook of Mathematical Functions: With Formulas, Graphs, and Mathematical Tables*, Dover Publications, New York, 1972.
17. Nabavi, M., M. H. K. Siddiqui, and J. Dargahi, "A new 9-point sixth-order accurate compact finite-difference method for the Helmholtz equation," *Journal of Sound and Vibration*, Vol. 307, 972–982, 2007.
18. Chang, H.-W., Y.-H. Wu, and W.-C. Cheng, "Hybrid FD-FD analysis of crossing waveguides by both the plus and the cross structural Symmetry," *Progress In Electromagnetics Research*, Vol. 103, 217–240, 2010.
19. Cheng, W.-C., "Finite-difference frequency-domain analysis of a dielectric waveguide crossing," Ph.D. Thesis, Department of Photonics, National Sun Yat-sen University, 2010.